ADVANCES IN MATERIALS SCIENCE, Vol. 24, No. 3 (81), September 2024

DOI: 10.2478/adms-2024-0019

Balázs Varbai[1, 2]*

[1]*Department of Materials Science & Engineering, Faculty of Mechanical Engineering, Budapest University of Technology and Economics, Budapest, Hungary*
[2]*MTA-BME Lendület "Momentum" High-performance Composite Metal Foams Research Group, Budapest, Hungary*

* *varbai.balazs@gpk.bme.hu*

SHIELDING GAS OXYGEN AND NITROGEN CONTENT EFFECTS IN THE CASE OF DUPLEX STAINLESS STEEL WELDING

ABSTRACT

The duplex stainless steels show improved localized corrosion resistance and strength comparing to the austenitic stainless steels. All of the duplex stainless steels solidify as pure ferrite and the double microstructure is evolving during the solid-state, diffusion driven phase transformation. In this research nitrogen and oxygen containing argon-based shielding gases were used. It was found that the nitrogen and oxygen addition significantly increased the weld metal austenite content, up to +27%. The oxygen addition also improved the weld dissolved oxygen content with up to +0.09%, and the weld penetration depth with up to +3.3 mm.

Keywords: *duplex stainless steel; gas tungsten arc welding; nitrogen; oxygen; austenite*

INTRODUCTION

Duplex stainless steels (DSS) show improved corrosion resistance and higher strength comparing to the conventional austenitic stainless steels grades [1, 2]. The improved properties are a result of the properly selected heat treatment, and chemical composition of DSS [3–5]. Comparing to the austenitic grades the DSSs have higher chromium (Cr) and lower nickel (Ni) contents [6, 7]. The pitting corrosion resistance is further improved by molybdenum (Mo) and nitrogen (N) addition. Among the DSSs the lean duplex (LDX) grades show a higher strength alternative to replace austenitic grades [8, 9]. In the LDX grades the lower Ni and Mo content is replaced by increased manganese (Mn) and N alloying, as these alloys are also austenite promoting elements.

The double, 1:1 austenite:ferrite phase ratio of DSSs and LDX grades is a result of solid-state phase transformation [10]. As all the DSSs and LDX grades solidify as ferrite, the ferrite-to-austenite phase transformation is mainly driven by the dissolved N atom diffusion, mainly under the 1200 to 800 °C cooling time ($\Delta t_{12/8}$) [11]. Thus, N alloying is an effective tool to promote austenite formation in the weld metal, and in the heat affected zone.

For the welding of DSS gas tungsten arc welding (GTAW) is an effective and widely used process, because GTAW results in clean, high-quality welds, less spattering, allowing welding in all positions [12]. For the GTAW of DSS another very significant advantage is that, the N-content of the weld metal can be influenced by the composition of the used

Received: 2024.08.17; Received in revised form: 2024.08.30; Accepted: 2024.09.03

shielding gas. Usually, ~2% of N_2 addition to the shielding gas is usually recommended to promote austenite formation in the weld metal, where the $\Delta t_{12/8}$ cooling time is usually very short. The N_2 in the shielding gas dissociates in the welding arc, and thus it can easily dissolve in the molten pool. After the solidification, the N atoms can diffuse to the interstitial free spaces in the face centered cubic lattice structure of the austenite phase, and thus N atoms promote austenite formation. The N_2 addition to the shielding gas is found to be an effective solution of austenite formation during different arc welding processes, mainly for gas tungsten arc welding (GTAW) [13–15].

For the GTAW of stainless steels oxygen addition to the molten pool is found to significantly increase weld penetration depth [16, 17]. The reason for this is that the forming oxide layer on the molten pool surface reverses the Marangoni-flow, resulting in an outward to inward motion, which increases the penetration depth [18, 19]. Beside applying oxide containing fluxes onto the surface prior to the welding (A-TIG method) [20, 21], it is also possible to add small amounts of oxygen to the shielding gas in the case of GTAW, to achieve the same effect.

Zou et al. [22] found that the weld penetration increased with the increase of the oxygen content in the case of GTAW of DSS grade SUS329J4L. They also verified that the weld depth/width ratio could be controlled by the oxygen content in the outer shielding gas. Zhang et al. [23] has found that oxygen mixing to the argon shielding gas dramatically increased the weld penetration depth in the case of GTAW of austenitic grade of SUS304, while the shielding gas did not have a significant effect on the microstructure of the weld metal. Pandya et al. [24] also found significant increase in the penetration depth by oxygen addition, in the case of GTAW of different stainless steels. Zou and Zhou [25] also used nitrogen and oxygen addition to argon based shielding gases to confirm that a small amount of active gas could improve the welding efficiency of the duplex stainless steel. Cross et al. [26] showed that oxygen in the shielding gas in amounts of 250 ppm could significantly increase the amount of weld metals nitrogen, particularly at low ambient pressures in the case of GTAW of DSS. Du Toit and Pistorius [27] found that the oxygen addition to the shielding gas can also reduce nitrogen loss from the molten pool during autogenous welding.

In this research, I used different, argon, nitrogen containing and oxygen containing shielding gases for the gas tungsten arc welding of LDX 2101 and LDX 2404 grades. The welds were evaluated by macro and micro examination, and pitting corrosion testing.

MATERIALS AND METHODS

Base materials

For the welding experiment lean duplex LDX 2101 and LDX 2404 grades were used in 3 mm thickness. The sample sizes were 150 × 50 × 3 mm. The chemical composition of the base materials (BM) can be seen in Table 1. The nitrogen and oxygen contents were measured by Horiba EMGA 620-W analyzer with combustion method. The rest of the alloying elements were measured by PMI Master Sort optical emission spectroscope. Both lean duplex grades have lower nickel and molybdenum content, and higher manganese and nitrogen content, compared to the conventional duplex grades, such as 2205. The higher Mn and N alloying tend to promote austenite formation during the ferrite-to-austenite solid-state phase transformation, which is retained by the very low Ni contents. The LDX 2404 grade has higher Cr, Mo, and N alloying, which improves the corrosion resistance and strength compared to the LDX 2101 grade. The oxygen content of the base materials was average 64 ± 18 ppm.

Table 1. *The chemical composition of the welded base materials*

Grade	Chemical composition (wt %)									
	C	Cr	Ni	Mn	Mo	N	Cu	Si	P	S	Fe
LDX 2101	0.02	21.5	1.5	4.9	0.3	0.234±0.002	0.3	0.66	0.03	0.001	bal.
LDX 2404	0.02	24.1	3.6	3.1	1.6	0.276±0.001	0.4	0.70	0.02	0.001	bal.

Welding parameters

For the welding experiments gas tungsten arc welding (GTAW) process was selected. The welding position was PA on the 150 × 50 × 3 mm sheets. The welding travel speed, torch angle, and arc length were kept constant by a self-made Yamaha type linear drive. The welding power source was an ESAB CaddyTIG 200. The used electrode was 2% CeO_2 added tungsten electrode in 2.6 mm diameter and grinded to a 40° tip angle. The polarity and the type of current was DC- (direct current, electrode on the negative side). The constant arc length was 3 mm, the torch angle was 90° with respect to the sheet surface. For the welding experiments argon (Ar) in 4.6 (99.996%) purity, premixed argon + 2% nitrogen (N_2) mixture, and oxygen bearing shielding gases were used. The oxygen (O_2) was mixed to the premixed argon + nitrogen shielding gas with a WITT type KM 20-3 gas mixer, which is capable of mixing argon-based gases with oxygen. The added oxygen amounts were +200 and +400 ppm. The shielding gas flow rate was 11 l/min in all cases. From the root side argon protection was used with 4 l/min flow rate in all cases. For the welding experiments 0.53 and 0.68 kJ/mm arc energies were used. The travel speed was constant 180 mm/min in all cases, and the welding currents were selected according to the different shielding gas types (different arc voltages) to keep the constant arc energies in all cases. For the welding experiment no filler materials have been used.

Macro and micro examination of the welds

The macro examination of the welds was done by Olympus SZX16 stereo microscope. For the weld penetration depth measurements standard metallographic samples were made. The welded sheets were first cut by a metallographic cutter with continuous cooling in order to prevent any microstructural changes. After that, the cross-sections were cold mounted in an epoxy resin, and grided up to 4000 grit papers. After grinding the mounted samples were polished with a polishing cloth and 3 μm grain size diamond paste. After the polishing the mounted welds were cleaned with ethanol and etched with Beraha II type (85 mL H_2O + 15 ml HCl + 1 g $K_2S_2O_5$) etchant. The etching times were 12-20 seconds of the different grades. This colour etching method tints the ferrite phase dark by sulphide decomposition, leaving the austenite phase light in all the metallographic images. For the microstructural examination Olympus PMG3 optical microscopy was used. The ferrite content was measured with Fischer type FMP3 Feritescope. The austenite contents were calculated as the measured ferrite content substituted from 100%.

Pitting corrosion testing

The pitting corrosion testing was done adoring to ASTM G48-A method. After the welding 25 × 25 × 3 mm samples were cut with the welded seam in the middle. First the samples were cleaned and degreased with acetone, and then each one of them was immersed into a 6% $FeCl_3$ solution in a 1-liter Erlenmeyer flask. The samples were fixed in a plastic sample holder to prevent crevice corrosion. The solution was 600 ml in all cases. The samples were kept at an average of 21 ± 2 °C temperature for 24 hours. After the immersion the samples were cleaned by ultrasonic cleaner and with plastic brushes in acetone. The weight of the samples before and after the test was measured by a Denver Instrument APX-200 type precision analytical balance, with 0.1 mg accuracy. The corrosion mechanism was also evaluated by Olympus SZX61 stereo microscopic technique.

RESULTS AND DISCUSSION

Results of the austenite content measurement in the weld metal

The metallographic images of the weld metals according to the arc energy and shielding gas type can be seen in Fig. 1. For the Ar welded samples, the microstructure shows dominantly ferritic microstructure with thin plates of grain boundary austenite (GBA) in all of the cases. The average ferrite grain sizes of the LDX 2101 and 2404 samples welded with 0.53 kJ/mm is 125 ± 15 μm, and 192 ± 28 μm for the 0.68 kJ/mm arc energy, respectively. The 2% N_2 addition increased the GBA plate with in all cases, and moreover in some of the samples intergranular austenite (IGA) promotion is also visible, most for the sample of LDX 2101 welded with 0.53 kJ/mm arc energy. The oxygen addition to the argon + nitrogen shielding gas mixture significantly increased the austenite content in the WM. It is visible on the metallographic images, that the IGA formation promoted inside the ferrite gains, increasing the total austenite content. From the microstructural images, the most increase is visible in the case of grade LDX 2404, welded with 0.68 kJ/mm arc energy.

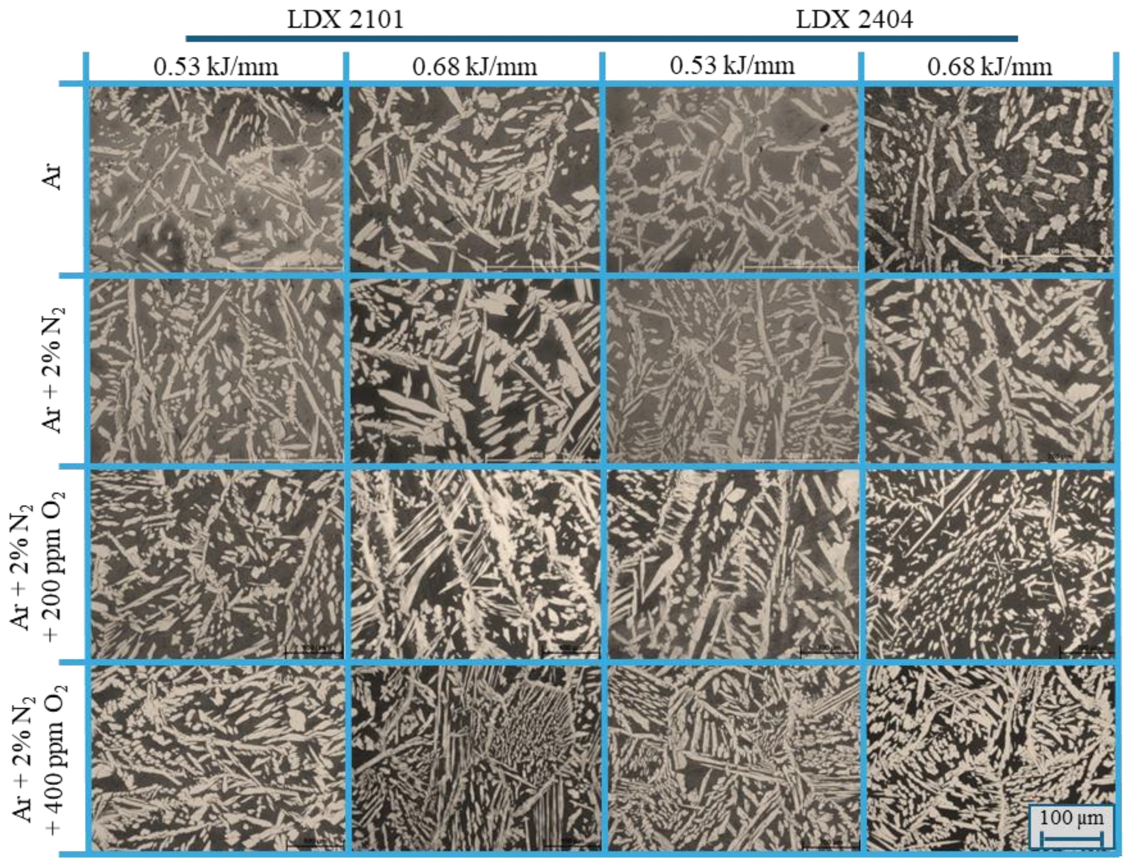

Fig. 1. The metallographic images of the weld metals according to the arc energy and shielding gas type

Fig. 2 shows the measured weld metal austenite contents according to the different shielding gas types and arc energies. From Fig. 2. it can generally be seen that the austenite content is increasing in the WM with the nitrogen and nitrogen + oxygen addition to the argon shielding gas. In the case of the argon welded samples the austenite content was measured in average of 27.0 ± 2% and 28.3 ± 2.2% in the case of grade LDX 2101, and 37.3 ± 1.9% and 34.6 ± 1.3% in the case of grade LDX 2404. The higher nickel (3.6%) and nitrogen (0.276%) content of the base material LDX 2404 resulted in lower nitrogen loss in the weld metal due to the evolution from the molten pool. The difference in arc energies had minor effect on the nitrogen loss in these cases. The 2% N_2 addition to the Ar shielding gas greatly increased the austenite content. This increase was more significant for the grade of LDX 2101, where the measured average austenite content was 36.9 ± 2.2% for the arc energy of 0.53 kJ/mm and 44.1 ± 1.3% for the arc energy of 0.68 kJ/mm. This means +37% and +56% austenite content increase in the weld metal, comparing to argon. The weld metal of grade LDX 2404 showed similar average austenite contents, 40.5 ± 1.5% for the arc energy of 0.53 kJ/mm and 38.3 ± 2% for 0.68 kJ/mm. The oxygen addition increased the austenite content in the WM in all of the cases. The greatest increase with the +200 ppm O_2 addition to the Ar + 2% N_2 shielding gas was measured in the case of grade LDX 2404 welded with 0.68 kJ/mm arc energy, where the average austenite content was 54.7 ± 1.8%. The +400 ppm O_2 addition further promoted the austenite formation. For the grade LDX 2101 the WM austenite contents were 51.1 ± 3.3% for the 0.53 kJ/mm arc energy, and 55.9 ± 3.4% for the 0.68 kJ/mm arc energy. For the grade LDX 2404 the WM austenite contents were 54.4 ± 1.2% for the 0.53 kJ/mm arc energy, and 60.7 ± 1.2% for the 0.68 kJ/mm arc energy. Overall, the 200 and 400 ppm oxygen addition further increased the austenite contents in all of the investigated weld metals, even compering to the argon + 2% nitrogen gas mixture. The possible reason for this is double. Once, the oxygen addition increases the thermal efficiency of the arc plasma, as the oxygen gas has higher thermal conductivity in the TIG welding arc temperature range, ~0.05W/cm°C, comparing to argons ~0.01 W/cm°C [28]. The higher thermal efficiency results in a higher effective heat input, which means longer $\Delta t_{12/8}$ cooling time for the ferrite-to-austenite phase transformation. Twice, the oxygen addition to the shielding forms an oxide layer on the molten pool surface, which reverses the Marangoni flow of the weld pool, resulting in an outward to inward flow direction. Thus, the nitrogen evolution (degassing) of the molten pool is less significant, and it helps in an even atomic nitrogen dissolution across the weld pool. The higher amount of dissolved nitrogen also promotes the austenite formation.

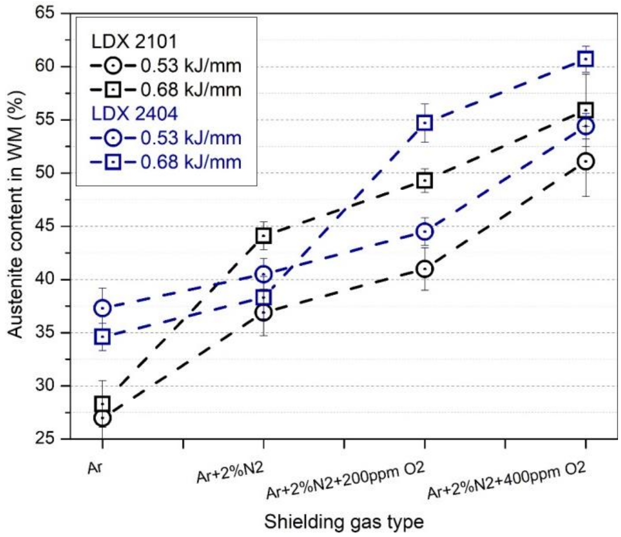

Fig. 2. The measured weld metal austenite contents according to the different shielding gas types and arc energies

Results of the weld nitrogen and oxygen content measurements

The results of the nitrogen content measurements in the weld metal can be seen in Fig. 3. according to the different gas types and arc energies. Using argon shielding gas resulted nitrogen loss in the molten pool is all cases. The nitrogen loss is more significant in the case of the higher, 0.68 kJ/mm arc energy. This means less austenite promoting elements in the weld metal, and thus more ferritic microstructure. The 2% nitrogen addition to the shielding gas evidently increased the nitrogen content in the weld metal, in all cases. Quantitatively, for the grade LDX 2101 the nitrogen content in the weld metal increased with +1% welded with 0.53 kJ/mm arc energy, and +4% welded with 0.68 kJ/mm arc energy. For the grade LDX 2404 this increase was +7% welded with 0.53 kJ/mm arc energy, and +5% welded with 0.68 kJ/mm arc energy. The +200 and +400 ppm oxygen addition remarkably increased the total nitrogen content in all of the weld metals. Quantitatively, comparing to the Ar + 2% N_2 gas mixture, the +200 ppm O_2 addition for the grade LDX 2101 increased the weld metal nitrogen content with +16% welded with 0.53 kJ/mm arc energy, and +30% welded with 0.68 kJ/mm arc energy. For the grade LDX 2404 this increase was +1% welded with 0.53 kJ/mm arc energy, and +17% welded with 0.68 kJ/mm arc energy. The +400 ppm O_2 addition for the grade LDX 2101 increased the weld metal nitrogen content with +32% welded with 0.53 kJ/mm arc energy, and +40% welded with 0.68 kJ/mm arc energy. For the grade LDX 2404 this increase was +9% welded with 0.53 kJ/mm arc energy, and +19% welded with 0.68 kJ/mm arc energy. From the results in can be concluded that the different grades acted differently to the oxygen addition to the shielding gas mixture. In the case of grade LDX 2101 the nitrogen content increase was much more prominent, compared to the grade LDX 2404. The reason for this is that the LDX 2404 has higher nitrogen alloying content in the base material, close to the solubility limit, thus the nitrogen dissolution is more retained in the molten pool. From Fig. 3. it is quantitatively visible, that the oxygen addition increased the nitrogen dissolution in the weld metal, due to the reversed Marangoni-flow.

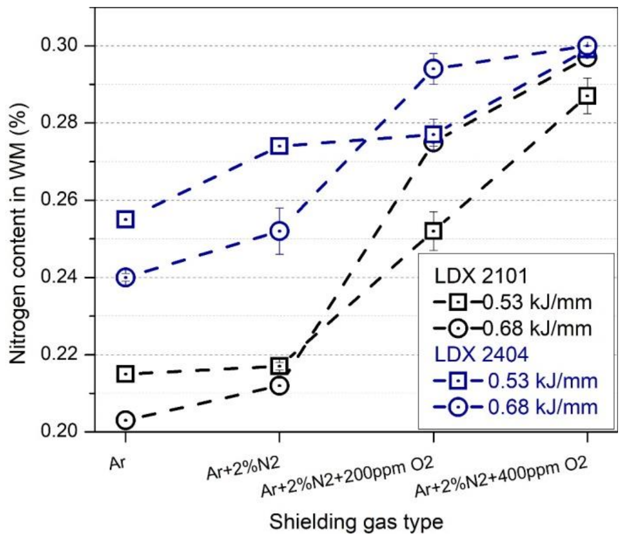

Fig. 3. The measured nitrogen content in the weld according to the different gas types and arc energies

Fig. 4. shows the weld metal oxygen content in the cases of oxygen bearing shielding gases. The dissolved oxygen content increased with the oxygen addition to the shielding gas. The highest oxygen content was measured for LDX 2101 grade welded with 0.68 kJ/mm arc energy and +400 ppm oxygen mixed to the shielding gas. In this case, the measured average total oxygen content was 420 ± 30 ppm. This high level of dissolved oxygen can deteriorate the ductility properties of the weld metal [29]. For the samples welded with 0.53 kJ/mm arc

energy the dissolved oxygen contents varied between 110 ± 20 ppm and 190 ± 20 ppm values. From the results it can be stated that, the oxygen addition to the shielding gas not only promoted the nitrogen dissolution, but also dissolved in the molten pool as oxygen atoms.

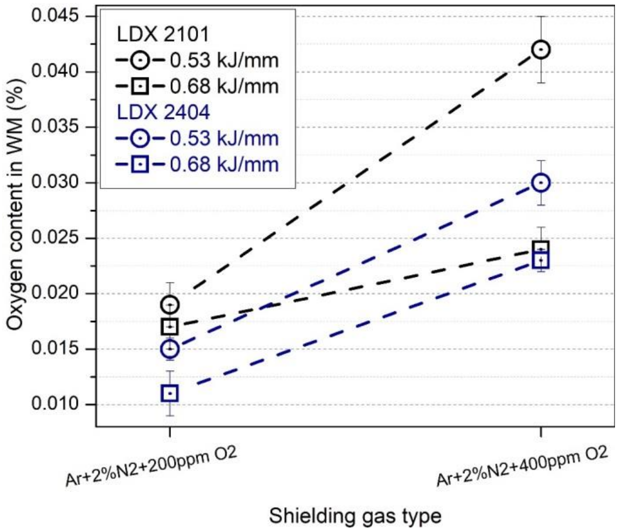

Fig. 4. The measured oxygen content in the weld according to the different gas types and arc energies

Results of the weld penetration depth measurements

The cross-section of different welds according to the shielding gas type and arc energies is visible in Fig. 5. In the case of argon shielding gas, very shallow and relatively wide welds can be seen, where the higher arc energy increased the penetration depth slightly. The nitrogen addition resulted in a minor increase in the penetration depth, however the further oxygen addition resulted in a significant increase in the weld area and penetration depth in all cases.

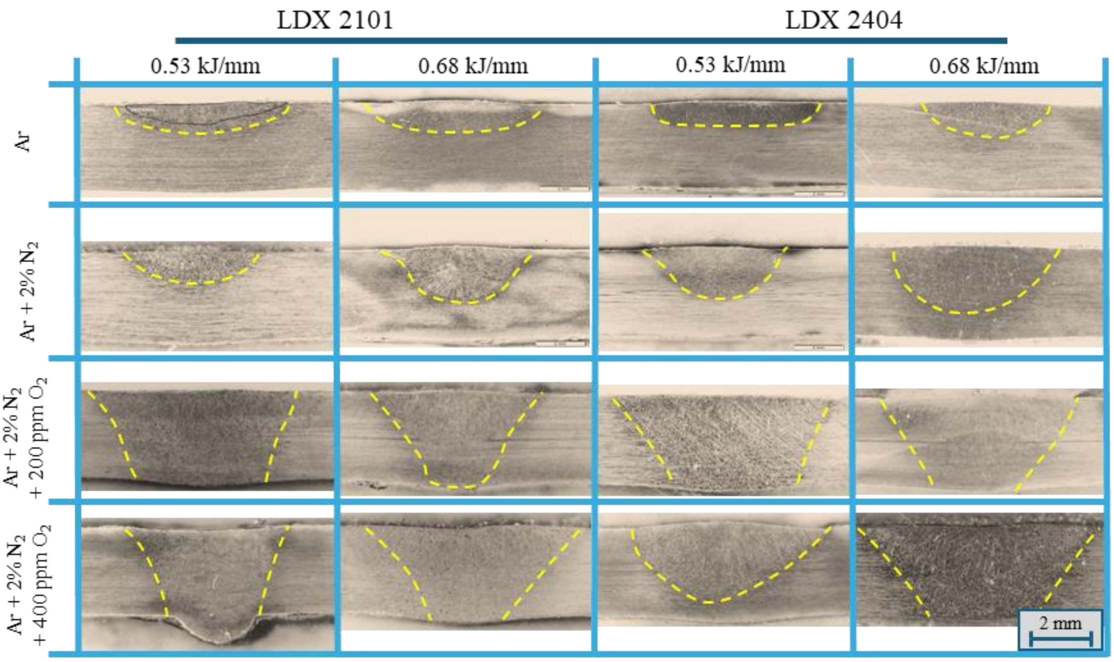

Fig. 5. The cross-section of different welds according to the shielding gas type and arc energies

The weld penetration depth according to the arc energy and shielding gas type can be seen in Fig. 6. It is visible, that the higher arc energy evidently results in deeper penetration in the case of argon welded samples. It is also visible, that the 2% nitrogen addition to the shielding gas practically did not improve the penetration depth. However, most importantly the +400 ppm oxygen addition had a great effect on the weld metal shape. Comparing to the Ar + 2% N_2 shielding gas, the +400 ppm oxygen addition increased the penetration depth from 0.6 to 3.92 mm (0.53 kJ/mm arc energy) and from 1.19 to 3.08 mm (0.68 kJ/mm arc energy) for the grade LDX 2101, and from 0.7 to 1.79 mm (0.53 kJ/mm arc energy) and from 1.7 to 3.04 mm (0.68 kJ/mm arc energy) for the grade LDX 2404. As described in the introduction section, the oxygen in the arc plasma reverses the Marangoni flow of the weld pool to an outward to inward motion, which deepens the penetration as more effective heat is absorbed through the cross-section of the pool. This phenomenon is the most advantageous property of the activated TIG welding process.

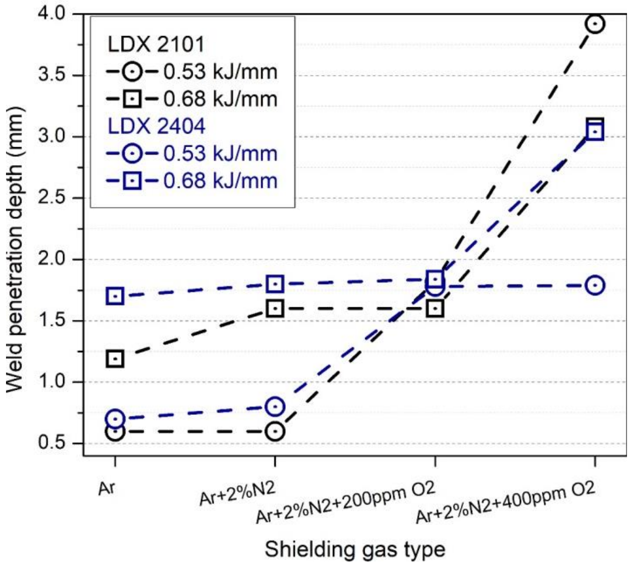

Fig. 6. The weld penetration depth according to the arc energy and shielding gas type

Results of the pitting corrosion testing

For the corrosion testing only the argon, argon + 2% nitrogen, and argon + 2% nitrogen + 200 ppm oxygen, welded with 0.53 kJ/mm samples were selected. The reason for this is that, only minor differences were found between the two used arc energies in the austenite and dissolved gas contents, and from practical standpoint it is more likely that the lower, +200 ppm oxygen content would be used during gas tungsten arc welding.

The face side of the welds before the corrosion test and after 24 hours immersion in 6% $FeCl_3$ solution can be seen in Fig. 7. From Fig. 7. it is visible, that the LDX 2101 grade showed lower corrosion resistance compared to grade LDX 2404 in all cases. The reason for this is the lower chromium, molybdenum and nitrogen content of grade LDX 2101, which means lower pitting resistance equivalent (PRE) numbers. For grade LDX 2101 the average PRE = 26, for LDX 2404 the average PRE = 33, where the PRE calculated using the formula: PRE = %Cr + 3.3×%Mo + 16×%N. Beside the base materials chemical composition, the shielding gas content also seems to have a significant effect on the corrosion resistance. For the grade LDX 2101 large, surface open pits are visible on the face side of the weld in the case of the argon and argon + 2% nitrogen welded samples. For the grade LDX 2404 minor, smaller sizes of pits are visible when these shielding gases were used. When oxygen was added to the gas mixture, less pits are visible in the case of both grades. It is also visible on the macro photos that the samples welded with oxygen bearing gases showed less oxide layer on the face side of the weld after the 24 hours of immersion and cleaning. The quantitative weight losses after the corrosion test can be seen in Table 2.

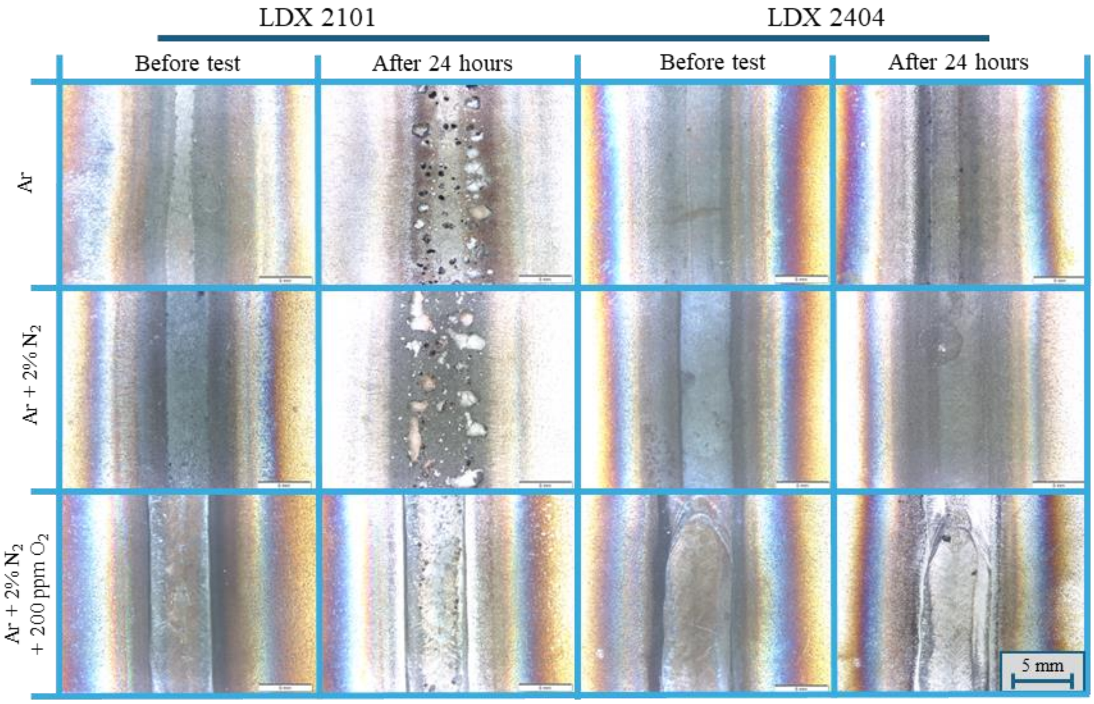

Fig. 7. The face side of the welds, welded with 0.53 kJ/mm arc energy, before the corrosion test and after 24 hours immersion in 6% $FeCl_3$ solution

Table 2. *The quantitative weight losses after the corrosion test*

Material grade	Shielding gas type	Weight before the test (g)	Weight after the 24h immersion (g)	Weight loss (%)
LDX 2101	Ar	23.7584	22.8716	-3.73
	Ar + 2% N_2	23.5341	22.6207	-3.88
	Ar + 2% N_2 + 200 ppm O_2	23.8714	23.8565	-0.06
LDX 2404	Ar	24.1000	24.0761	-0.10
	Ar + 2% N_2	22.2507	22.2363	-0.06
	Ar + 2% N_2 + 200 ppm O_2	21.4567	21.4515	-0.02

For the grade LDX 2101 the average weight loss was ~4% when welded with argon and argon + nitrogen mixture. When oxygen was added to the shielding gas, this weight loss was negligible. For the grade LDX 2404 all of the weight loss values were very minor. However, for both of the grades it is visible that, the minimum weight losses were measured in the case of the samples welded with the oxygen containing shielding gas. The possible reason for this is that, the oxygen addition to the shielding gas promoted an oxide layer formation on the molten pool surface, which later protected the weld metal from further oxidation. This is the reason why the oxygen welded samples show shinier weld face surfaces after the corrosion tests and cleaning, because the corrosion mechanism took place on the previously formed oxide layer. This result is also confirmed by Brytan and Niagaj [30]. In their research it was also found that, the LDX 2404 lean duplex stainless steel welds obtained with A-TIG process has a much lower tendency to pitting corrosion than traditional welds made by TIG (GTAW) method.

It is worth to mention that the samples were investigated in as welded condition, to examine the effects of the different shielding gas types. In industrial circumstances the welds should be cleaned after welding (e.g. with pickling) and the passive chromium-oxide layer should be rebuilt by passivation. In those circumstances, the welds would probably show different resistances to pitting corrosion.

CONCLUSIONS

In this research the effects of different, argon, nitrogen, and oxygen containing shielding gases were investigated in the case of gas tungsten arc welding of lean duplex grades LDX 2101 and LDX 2404. From the results, the following conclusions can be drawn:

– The nitrogen and oxygen addition to the argon shielding gas increased the austenite content in the weld metal in all cases. The highest austenite contents were measured in the case of grade LDX 2404; 54.4 ± 1.2% for the 0.53 kJ/mm arc energy, and 60.7 ± 1.2% for the 0.68 kJ/mm arc energy.
– Both the nitrogen and oxygen addition to the argon shielding gas increased the total dissolved nitrogen content in the weld metal in all cases. The highest nitrogen contents were measured in the case of +400 ppm oxygen addition to the shielding gas, where the dissolved total nitrogen content varied between 0.287 ± 0.005 and 0.3 ± 0.002%. The +200 and +400 ppm oxygen addition to the shielding gases also increased the dissolved oxygen content to the weld metal with the maximum value of 420 ± 30 ppm.
– The oxygen addition to the shielding gas significantly increased the weld penetration depths. Comparing to the Ar + 2% N_2 shielding gas, the +400 ppm oxygen addition increased the penetration depth from 0.6 to 3.92 mm (0.53 kJ/mm arc energy) and from 1.19 to 3.08 mm (0.68 kJ/mm arc energy) for the grade LDX 2101, and from 0.7 to 1.79 mm (0.53 kJ/mm arc energy) and from 1.7 to 3.04 mm (0.68 kJ/mm arc energy) for the grade LDX 2404.
– During the pitting corrosion testing the LDX 2404 showed superior corrosion resistance compared to the grade LDX 2101 in all cases. The lowest weight losses were measured in the case of using oxygen bearing shielding gases, where the oxide layer formed on the molten pool during welding protected the weld metal from further oxidation.
– The results confirmed that the +200 or +400 ppm oxygen addition to the argon + 2% nitrogen shielding gas can significantly increase the austenite and dissolved nitrogen content of the weld metal, and the penetration depth in the case of gas tungsten arc welding.

ACKNOWLEDGEMENT

This paper has been supported by the National Research, Development and Innovation Office – NKFIH, OTKA PD 138729.

Conflicts of Interest

The author declare that they have no competing financial interests or personal relationships that could have seem to influence the study reported in this paper.

REFERENCES

1. Landowski M (2019) Influence of Parameters of Laser Beam Welding on Structure of 2205 Duplex Stainless Steel. Advances in Materials Science 19:21–31. https://doi.org/10.2478/adms-2019-0002
2. Maurya AK, Pandey SM, Chhibber R, Pandey C (2023) Structure–property relationships and corrosion behavior of laser-welded X-70/UNS S32750 dissimilar joint. Archives of Civil and Mechanical Engineering 23:81. https://doi.org/10.1007/s43452-023-00627-5
3. Łabanowski J, Świerczyńska A, Topolska S (2015) Effect of Microstructure on Mechanical Properties and Corrosion Resistance of 2205 Duplex Stainless Steel. Polish Maritime Research 21:108–112. https://doi.org/10.2478/pomr-2014-0047
4. Landowski M, Świerczyńska A, Rogalski G, Fydrych D (2020) Autogenous Fiber Laser Welding of 316L Austenitic and 2304 Lean Duplex Stainless Steels. Materials 13:2930. https://doi.org/10.3390/ma13132930
5. Quackatz L, Gornushkin I, Griesche A, et al (2024) In situ chemical analysis of duplex stainless steel weld by laser induced breakdown spectroscopy. Spectrochimica Acta Part B: Atomic Spectroscopy 214:106899. https://doi.org/10.1016/j.sab.2024.106899
6. Májlinger K, Szabó PJ (2011) Effect of grain boundary structure on the intercrystalline damaging of austenic steel during brazing. Periodica Polytechnica Mechanical Engineering 55:105. https://doi.org/10.3311/pp.me.2011-2.08
7. SZCZUCKA-LASOTA B, WĘGRZYN T (2024) Welding of 1.4462 duplex steel used in means of road transport. Scientific Journal of Silesian University of Technology Series Transport 122:281–292. https://doi.org/10.20858/sjsutst.2024.122.15
8. Dobránszky J, Mészáros I, Nagy G (2000) Mechanical and thermal induced phase transformations in superduplex stainless steel. 6th World Duplex Conference and Expo 385–393
9. Bassani P, Breda M, Brunelli K, et al (2013) Characterization of a Cold-Rolled 2101 Lean Duplex Stainless Steel. Microscopy and Microanalysis 19:988–995. https://doi.org/10.1017/S1431927613001426
10. Köse C, Topal C (2022) Texture, microstructure and mechanical properties of laser beam welded AISI 2507 super duplex stainless steel. Materials Chemistry and Physics 289:126490. https://doi.org/10.1016/j.matchemphys.2022.126490
11. Westin EM, Westerberg LG (2024) Evaluation of methods used for simulation of heat-affected zones in duplex stainless steels. Welding in the World 68:1941–1963. https://doi.org/10.1007/s40194-024-01698-5
12. da Silva NN, Ribeiro PH, Moreno AM, et al (2018) Study on the electric arc of GTAW process. Journal of Physics: Conference Series 1126:012013. https://doi.org/10.1088/1742-6596/1126/1/012013
13. Bobadilla M, Tschiptschin A, Bobadilla M, Tschiptschin A (2015) On the Nitrogen Diffusion in a Duplex Stainless Steel. Materials Research 18:390–394. https://doi.org/10.1590/1516-1439.337714

14. Pimenta AR, Diniz MG, Perez G, Solórzano-Naranjo IG (2020) Nitrogen Addition to the Shielding Gas for Welding Hyper-duplex Stainless Steel. Soldagem & Inspeção 25:1–8. https://doi.org/10.1590/0104-9224/si25.12
15. Orłowska M, Pańcikiewicz K, Świerczyńska A, Landowski M (2023) Kinetics of Intermetallic Phase Precipitation in Manual Metal Arc Welded Duplex Stainless Steels. Materials 16:7628. https://doi.org/10.3390/ma16247628
16. Dobránszky J, Sándor T, Nagy-Hinst A, et al (2007) Weld Pool Characteristics of the ATIG-Welded Joints. In: Duplex 2007: International Conference and Expo. Grado, Italy
17. Sándor T, Dobránszky J (2008) ATIG welding of duplex steel. Materials Science Forum 589:49–54
18. Sándor T, Mekler C, Dobránszky J, Kaptay G (2013) An Improved Theoretical Model for A-TIG Welding Based on Surface Phase Transition and Reversed Marangoni Flow. Metallurgical and Materials Transactions A 44:351–361. https://doi.org/10.1007/s11661-012-1367-2
19. Lu S, Fujii H, Nogi K (2008) Marangoni convection and weld shape variations in He–CO2 shielded gas tungsten arc welding on SUS304 stainless steel. Journal of Materials Science 43:4583–4591. https://doi.org/10.1007/s10853-008-2681-3
20. Touileb K, Hedhibi AC, Djoudjou R, et al (2022) Mechanical, Microstructure, and Corrosion Characterization of Dissimilar Austenitic 316L and Duplex 2205 Stainless-Steel ATIG Welded Joints. Materials 15:2470. https://doi.org/10.3390/ma15072470
21. Tathgir S, Rathod DW, Batish A (2019) A-TIG welding process for enhanced-penetration in Duplex stainless-steel: effect of activated fluxes. Materials and Manufacturing Processes 00:1–12. https://doi.org/10.1080/10426914.2019.1666990
22. Zou Y, Ueji R, Fujii H (2014) Effect of oxygen on weld shape and crystallographic orientation of duplex stainless steel weld using advanced A-TIG (AA-TIG) welding method. Materials Characterization 91:42–49. https://doi.org/10.1016/j.matchar.2014.02.006
23. Zhang J, Shao P, Wang X, Fan D (2023) Improving weld penetration by two-TIG arc activated via mixing oxygen into shielding gas. The International Journal of Advanced Manufacturing Technology 125:169–181. https://doi.org/10.1007/s00170-022-10703-4
24. Pandya D, Badgujar A, Ghetiya N (2021) A novel perception toward welding of stainless steel by activated TIG welding: a review. Materials and Manufacturing Processes 36:877–903. https://doi.org/10.1080/10426914.2020.1854467
25. Zou Y, Zhou X (2023) Effects of Nitrogen-Added Double Shielding Gas and Solution Treatment on Duplex Stainless Steel Weld Microstructure of Deep-Penetration Tungsten Inert Gas Welding. Journal of Materials Engineering and Performance 32:6995–7003. https://doi.org/10.1007/s11665-022-07594-7
26. Cross CE, Hoffmeister H, Huismann G (1997) Nitrogen control in hyperbaric welding of duplex stainless steel. Welding in the World / Le Soudage dans le Monde 39:154–161
27. Du Toit M, Pistorius PC (2009) Shielding Gas Oxygen Additions as a Means of Curbing Nitrogen Degassing during the Autogenous Arc Welding of Nitrogen-Alloyed Stainless Steel. Welding in the World 53:38–47. https://doi.org/10.1007/BF03266690
28. Suban M, Tušek J, Uran M (2001) Use of hydrogen in welding engineering in former times and today. Journal of Materials Processing Technology 119:193–198. https://doi.org/10.1016/S0924-0136(01)00956-6
29. Zou Y, Ueji R, Fujii H (2015) Mechanical properties of advanced active-TIG welded duplex stainless steel and ferrite steel. Materials Science and Engineering: A 620:140–148. https://doi.org/10.1016/j.msea.2014.10.006

30. Brytan Z, Niagaj J (2016) Corrosion Resistance and Mechanical Properties of TIG and A-TIG Welded Joints of Lean Duplex Stainless Steel S82441 / 1.4662. Archives of Metallurgy and Materials 61:771–784. https://doi.org/10.1515/amm-2016-0131